Intermetallics 109 (2019) 167–173

Contents lists available at ScienceDirect

Intermetallics

journal homepage: www.elsevier.com/locate/intermet

Evaluating elastic properties of a body-centered cubic NbHfZrTi high-entropy alloy – A direct comparison between experiments and *ab initio* calculations

Y.X. Ye[a], B.L. Musico[a], Z.Z. Lu[a], L.B. Xu[a], Z.F. Lei[b], V. Keppens[a], H.X. Xu[a], T.G. Nieh[a,c,*]

[a] Department of Materials Science and Engineering, University of Tennessee, Knoxville, TN 37996, USA
[b] State Key Laboratory for Advanced Metals and Materials, University of Science and Technology Beijing, Beijing 100083, China
[c] Institute for Advanced Study/Department of Materials Science and Engineering, City University of Hong Kong, Hong Kong, China

ARTICLE INFO

Keywords:
High-entropy alloy
Elastic properties
Elastic anisotropy
Resonant ultrasound spectroscopy (RUS)
Density functional theory

ABSTRACT

In this study, elastic constants of the equiatomic body-centered cubic NbHfZrTi high-entropy alloy (HEA) were experimentally evaluated using resonant ultrasound spectroscopy and compared directly with calculations based on density functional theory. Elastic properties, including Young's modulus, shear modulus, bulk modulus, Poisson's ratio, and Debye temperature, of polycrystalline aggregates were obtained from measurements and calculations, and excellent agreement was found between the experimental and theoretical data. We also made efforts to employ the rule-of-mixtures (ROM) to predict the elastic moduli of the current alloy, as well as other HEAs reported in the literature, and found that the lower-bound prediction provided a reasonable estimate of the elastic moduli of single-phase HEAs.

1. Introduction

Recently developed high-entropy alloys (HEAs) have triggered extensive research efforts and attempts to broaden the compositional space of alloy design [1–3]. Different from traditional alloys, which are composed of one major element with some additional minor elements, HEAs consist of multiple principal metallic elements in equiatomic or nearly equiatomic ratio. This new class of alloys has high configurational entropy and favors the formation of simple solution-like structures, such as face-centered cubic (FCC) [4–6] and body-centered cubic (BCC) [7–9], rather than complex ordered intermetallics. These HEAs have demonstrated some unusual mechanical and physical properties, such as excellent combination of strength and ductility [10,11], good resistance to high-temperature softening [8] and fracture [4], attractive tribological properties [12], and outstanding magnetic properties [13].

Elastic moduli are one of the intrinsic material properties, which directly affect various fundamental properties such as mechanical and thermal properties [14]. For example, they govern the stress-strain relation before yielding, and the shear modulus is closely related to dislocation motion on slip planes, thus contributing to strengthening and ductility. Elastic properties are also linked to the melting point, thermal expansion and Debye temperatures. There have been several theoretical investigations of elastic properties of HEAs [15–21]. For example, alloying effects on elastic properties were explored in FCC-structured Cantor alloy (i.e., NiCrMnFeCo) and its subsystems [15,16]; studies have also been carried out on various BCC-structured refractory HEAs using different *ab initio* based calculations, including virtual crystal approximation (VCA), coherent potential approximation (CPA) and special quasi-random structure (SQS) [17–19]. However, experimental measurements of elastic properties of HEAs are still relatively limited, especially for BCC-structured HEAs [7,22]. In fact, many studies were cross-referenced, namely, theoretical and experimental works were carried out by different groups, data comparisons were made, nonetheless. A direct comparison between experimental measurements and theoretical calculations has not yet been made for HEAs. In this paper, we perform both resonant ultrasound spectroscopy (RUS) experiments and density functional theory (DFT) calculations to evaluate the elastic properties of a BCC-structured NbHfZrTi HEA and provide a direct comparison to validate the calculations. Additionally, the applicability of the simple rule-of-mixtures (ROM) to equiatomic solid solution alloys is also explored and discussed.

2. Methods

2.1. Experimental procedure

The equiatomic NbHfZrTi HEA was synthesized, as described in

* Corresponding author. Department of Materials Science and Engineering, University of Tennessee, Knoxville, TN 37996, USA.
E-mail address: tnieh@utk.edu (T.G. Nieh).

https://doi.org/10.1016/j.intermet.2019.04.003
Received 6 December 2018; Received in revised form 23 February 2019; Accepted 1 April 2019

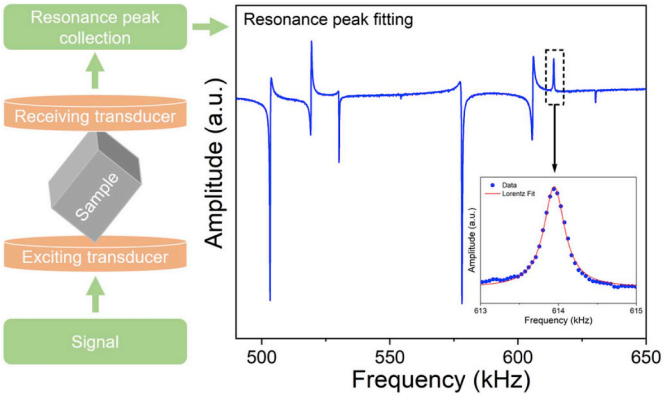

Fig. 1. Schematic diagram for RUS measurement setup and a typical RUS resonance spectrum (in-phase signal amplitude vs. frequency) of NbHfZrTi HEA with an inset showing the Lorentz fitting of a selected peak.

previous papers [9,12]. The alloy was arc-melted, drop cast, homogenized, cold rolled with 80% reduction in thickness, and then fully annealed to obtain a recrystallized, equiaxed microstructure with a grain size of ~150 μm. X-ray diffraction (XRD) and transmission electron microscopy (TEM) results have shown that the present alloy has a single-phase BCC structure with a lattice parameter of 3.444 Å [9,12].

Elastic constants were measured using resonant ultrasound spectroscopy (RUS). A rectangular parallelepiped sample was corner mounted between two transducers as schematically illustrated in Fig. 1. Utilizing the mechanical resonances of a material, RUS uses sample dimensions and resonances to fit the experimentally collected resonances to a calculated spectrum based on estimated elastic moduli, using an iteratively inverse fitting process [23]. The elastic constants C_{ij} were determined from ~40 resonances with frequency ranging from 200 to 1000 kHz. A typical RUS resonance spectrum obtained from the current NbHfZrTi HEA is shown in Fig. 1, in which the inset shows an example of Lorentz fitting of a single resonance peak. In the absence of texture, elastic isotropy was assumed in the polycrystalline specimen. The density of the annealed alloy was measured using a Denver Instrument SI-234 device.

2.2. Computational methodology

Kohn-Sham density functional theory [24,25] simulations were performed to calculate the elastic constants of the alloy using Vienna *Ab initio* Simulation Package (VASP) [26,27], in which the projector-augmented wave (PAW) method [28] was employed. The exchange-correlation functional in the framework of Perdew-Burke-Ernzerhof (PBE) [29] was used. Special quasi-random structures (SQSs) [30] were generated via the mcsqs [31] program in the Alloy-Theoretic Automated Toolkit (ATAT) [32,33], and were utilized in the calculations in order to achieve statistically better results due to the vast configuration space of the alloys. Specifically, 3 SQSs of 4 × 4 × 4 supercell size in the unit of conventional BCC unit cell were tested (Fig. 2). For each configuration, its lattice parameter was optimized before the elastic constant calculation while allowing the ionic relaxation till the Hellmann-Feynman force is smaller than 0.01 eV/Å on each atom. The average lattice constant of the 3 SQSs was found to be 3.428 Å, which agrees well with our previous experimental result of 3.444 Å [9]. The elastic constants were then derived from the relaxed structures by calculating the stress-strain relationship through a finite difference approach with a displacement size of 0.1 Å [34,35]. The results obtained for each SQS (compiled in Table 1) exhibit lower symmetry than the theoretical cubic ones due to the limited supercell size; hence we take the arithmetic average among the supposedly equivalent terms for C_{11}, C_{12}, and C_{44}, respectively. The calculated properties were further averaged among the 3 SQSs and summarized in Table 2. Our results indicate that the modulus calculations are robust against different SQSs with the relative standard deviations being 1.2%, 1.6%, and 7.6% for C_{11}, C_{12}, and C_{44}, respectively. For all the simulations, the energy cut-off for plane-wave basis was set as 500 eV while the Brillouin zone was sampled by a 2 × 2 × 2 mesh. Electronic convergence criterion was set to be 10^{-5} eV.

3. Results and discussion

The three single-crystal elastic constants C_{11}, C_{12} and C_{44} of the present NbHfZrTi HEA calculated from DFT and the two polycrystalline moduli determined from RUS are listed in Table 2. It is noted that for polycrystals with only two independent elastic constants, C_{12} is constrained by the equation $C_{44} = (C_{11} - C_{12})/2$. The calculated single-crystal elastic constants are noted to satisfy the Born dynamical stability criteria for cubic systems [20,36], namely, $C_{11} + 2C_{12} > 0$, $C_{11} > |C_{12}|$ and $C_{44} > 0$. Thus, the current NbHfZrTi HEA is expected to be mechanically stable.

Use the single-crystal elastic constants, the polycrystalline elastic properties (specifically, bulk modulus B, shear modulus G, Young's modulus E, and Poisson's ratio ν) can be estimated according to Voigt-Reuss-Hill (VRH) averaging approximations [37]. The shear modulus can be subsequently obtained from

$$G = \frac{(G_V + G_R)}{2} \tag{1}$$

where G_V and G_R are Voigt and Reuss shear moduli, respectively, representing the upper and lower limit of the polycrystalline moduli, given by

$$G_V = \frac{(C_{11} - C_{12}) + 3C_{44}}{5} \text{ and } G_R = \frac{5(C_{11} - C_{12})C_{44}}{3(C_{11} - C_{12}) + 4C_{44}} \tag{2}$$

B, E and ν are calculated from the following equations

$$B = \frac{C_{11} + 2C_{12}}{3} \tag{3}$$

$$E = \frac{9BG}{3B + G} \tag{4}$$

$$\nu = \frac{3B - 2G}{6B + 2G} \tag{5}$$

The polycrystalline moduli (B, G, E and ν) of the current NbHfZrTi HEA deduced from Eqs. (1)–(5) by inserting RUS measurements and DFT calculations are summarized in Table 2. It is clearly seen that DFT and RUS results display excellent consistency within 6% difference for all polycrystalline moduli.

The above elastic properties also allow us to predict the brittle/ductile characteristic of a material in light of Pugh's ratio (B/G) [38], Poisson's ratio ν, and Cauchy pressure ($CP = C_{12} - C_{44}$) [39]. In principle, bulk modulus B reflects the bonding strength between atoms and the resistance to cleavage, whereas the shear modulus G describes the resistance against dislocation movement. A high Pugh's ratio with $B/G > 1.75$ generally implies a ductile material ($B/G < 1.75$ indicates brittle behavior) [38]. For polycrystals, the Poisson's ratio ν is actually connected to the B/G ratio by recasting Eq. (5) as $\nu = (3B/G - 2)/(6B/G + 2)$, which yields a critical value of 0.26 for the brittle/ductile transition. It is clearly seen from Table 2 that B/G values range from 4.2 to 4.6 and the Poisson's ratio ν ~0.39, determined by RUS experiments and DFT calculations, both predict ductile nature of the present HEA. In addition, Cauchy pressure (CP), which relates to the angular character of atomic bonding, is often indicative of ductility and, in fact, a negative CP corresponds to covalent bond accompanied with brittle behavior, and a positive CP stands for more metallic character and tendency toward ductility [39]. The present NbHfZrTi HEA exhibits a large positive CP value (Table 2), suggesting it is a ductile alloy. In summary, all relevant elastic parameters indicate that the present HEA

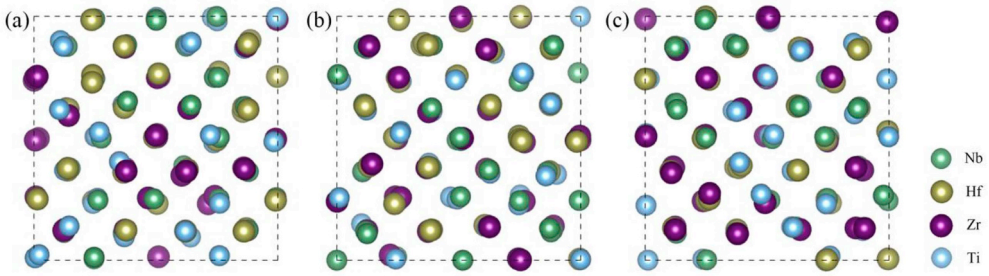

Fig. 2. Side view of the atomistic configurations of the three SQSs used to model NbHfZrTi HEA.

Table 1
Non-zero elastic constants (in GPa) of the 3 SQSs.

SQS No.	C_{11}	C_{22}	C_{33}	C_{12}	C_{13}	C_{23}	C_{44}	C_{55}	C_{66}
1	135.7	136.1	133.2	99.5	102.6	99.8	31.1	25.3	32
2	138.1	132.6	134.8	98.6	98.4	103.1	31.5	32	31
3	135.6	135.5	134.8	100.3	100.4	100.9	28.7	32.2	28.5

Table 2
Comparison of elastic constants and polycrystalline moduli of NbHfZrTi HEA between RUS measurements and DFT calculations. The percentage differences between DFT calculations and RUS measurements are shown in the parenthesis.

Methods	C_{11} (GPa)	C_{12} (GPa)	C_{44} (GPa)	CP (GPa)	A_z	E (GPa)	G (GPa)	B (GPa)	ν	B/G
RUS	139.2	89.0	25.1	63.9	\	69.7	25.1	105.7	0.390	4.2
DFT	135.1	100.4	30.2	70.2	1.74	67.7 (−3%)	24.2 (−4%)	112.0 (6%)	0.399 (2%)	4.6

would be ductile with a high room-temperature tensile ductility, which is consistent with the experimental observation (ductility ~15%) [40].

Elastic anisotropy can affect various mechanical behavior, such as micro-cracking and the incipient plasticity in materials [41,42]. It is, therefore, pertinent to evaluate the elastic anisotropy of the current HEA. Elastic anisotropy is usually described by the Zener anisotropy ratio, $A_Z = 2C_{44}/(C_{11} - C_{12})$, in which $A_Z = 1$ corresponds to elastic isotropy and any departure from unity indicates the degree of elastic anisotropy [21,36]. In Table 2, it can be observed that our DFT calculation predicts $A_z = 1.74$. It is noted, however, only isotopically polycrystalline samples are available for the RUS measurements, which prohibits us from directly verifying the above calculations. In order to further visualize the anisotropic characteristics, the three-dimensional (3D) distributions of Young's modulus E, shear modulus G, bulk modulus B and Poisson's ratio ν based on our DFT results are plotted in Fig. 3. Equations used for evaluating the elastic properties in any arbitrary crystallographic direction [hkl] for cubic systems are given as [36,43,44].

$$1/E = S_{11} - 2(S_{11} - S_{12} - S_{44}/2)(l_1^2 l_2^2 + l_2^2 l_3^2 + l_3^2 l_1^2) \quad (6)$$

$$1/G = S_{44} + 4(S_{11} - S_{12} - S_{44}/2)(l_1^2 l_2^2 + l_2^2 l_3^2 + l_3^2 l_1^2) \quad (7)$$

$$1/B = 3(S_{11} + 2S_{12}) \quad (8)$$

$$\nu = -\frac{S_{12} + (S_{11} - S_{12} - S_{44}/2)(l_1^2 l_2^2 + l_2^2 l_3^3 + l_3^2 l_1^2)}{S_{11} - 2(S_{11} - S_{12} - S_{44}/2)(l_1^2 l_2^2 + l_2^2 l_3^2 + l_3^2 l_1^2)} \quad (9)$$

where $S_{11} = (C_{11} + C_{12})/[(C_{11} - C_{12})(C_{11} + 2C_{12})]$, $S_{12} = -C_{12}/[(C_{11} - C_{12})(C_{11} + 2C_{12})]$ and $S_{44} = 1/C_{44}$ are elastic compliances, and l_1, l_2, l_3 are the direction cosines. In Fig. 3, it is observed that Young's modulus, shear modulus, and Poisson's ratio exhibit orientation-dependence and thus anisotropy, whilst the bulk modulus is a perfect sphere since it is always isotropic for the cubic system. It is noted that, whereas E has its highest (lowest) value along < 111 > (< 100 >) directions with a descending order of $E_{111} > E_{110} > E_{100}$, G and ν show a completely opposite trend. The orientation dependence of elastic modulus can be also described as a function of θ, where θ denotes the angle between the < 100 > direction and a certain crystal direction on the {110} planes. Some crystal directions corresponding to θ angles are marked on the top axis of Fig. 4a. For the present NbHfZrTi HEA, since Nb is the only constituent element with a BCC structure, we plot the Young's moduli of the two materials together in Fig. 4a for easy comparison (elastic constants of Nb are from Ref. [45]). It is particularly noted that Nb displays an opposite trend against NbHfZrTi, namely, Nb has its highest (lowest) value along < 100 > (< 111 >) directions with a descending order of $E_{100} > E_{110} > E_{111}$. Moreover, it is readily seen from Fig. 4a that Young's moduli along < 100 > direction highly differ between pure Nb and the current NbHfZrTi HEA, i.e., 151.5 vs 49.5 GPa which can be rationalized as follows. Combined with Zener anisotropy ratio, Eq. (6) for Young's modulus in an arbitrary direction can be recast as $1/E = S_{11} - (A_Z - 1)S_{44}(l_1^2 l_2^2 + l_2^2 l_3^2 + l_3^2 l_1^2)$. If the Zener anisotropy ratio $A_Z < 1$, i.e., (A_Z - 1) is negative, Young's modulus would have its maximum value in the < 100 > direction and minimum value in the < 111 > direction; by contrast, if the Zener anisotropy ratio $A_Z > 1$, i.e., (A_Z - 1) is positive, Young's modulus would be a minimum in the < 100 > and maximum in the < 111 > direction. The present NbHfZrTi HEA and pure Nb have a Zener ratio of $A_Z^{HEA} = 1.74 > 1$ and $A_Z^{Nb} = 0.51 < 1$, respectively, resulting in an opposite trend and largest difference in Young's moduli along the < 100 > direction. The opposite anisotropy can be verified on the basis of electron configurations. It is generally recognized that the average valence electrons per atom (e/a ratio) in the free atom configuration is a dominant factor in controlling the elastic properties (e.g., elastic anisotropy) of BCC transition metals and alloys [46–48]. The Zener anisotropy ratio for pure Nb and the current NbHfZrTi HEA as a function of e/a ratio is plotted in Fig. 4b, in which values for some BCC transition alloys from literature [46–53] are also included for comparison. It is clearly observed that the Zener anisotropy ratio decreases with the increase of e/a ratio, and particularly an e/a ratio of ~4.7 would predict an elastic anisotropy of $A_Z = 1$. The present HEA and pure Nb have their e/a ratios of 4.25 and 5, resulting

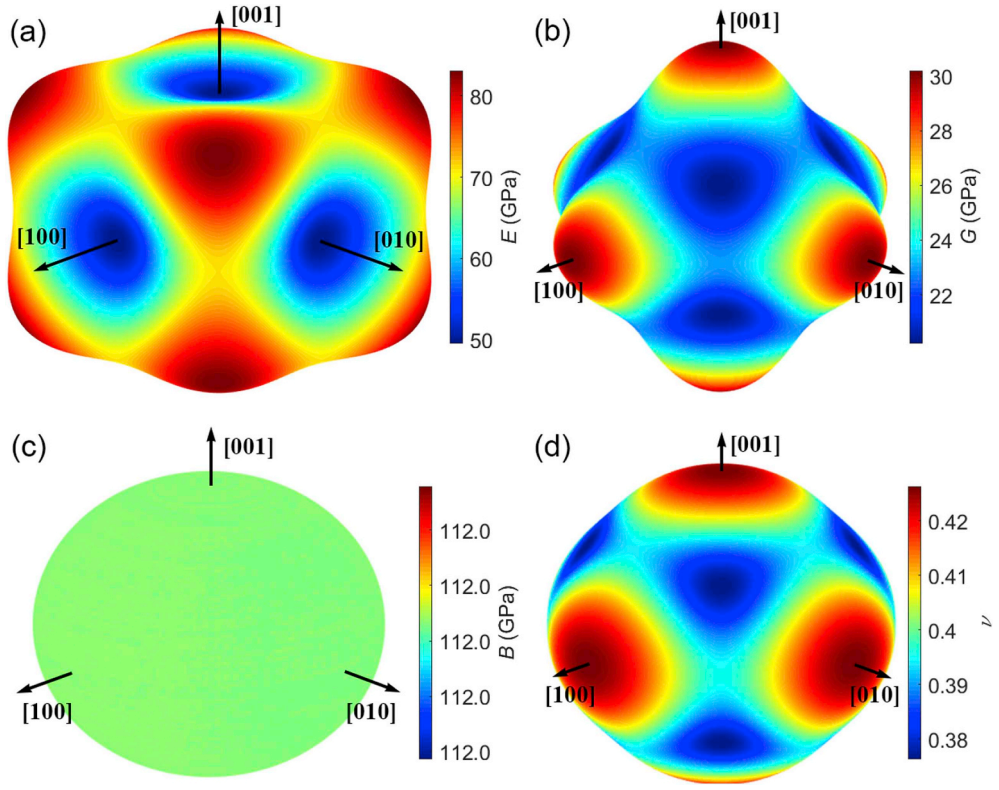

Fig. 3. 3D visualizations of (a) Young's modulus, (b) shear modulus, (c) bulk modulus, and (d) Poisson's ratio of NbHfZrTi HEA.

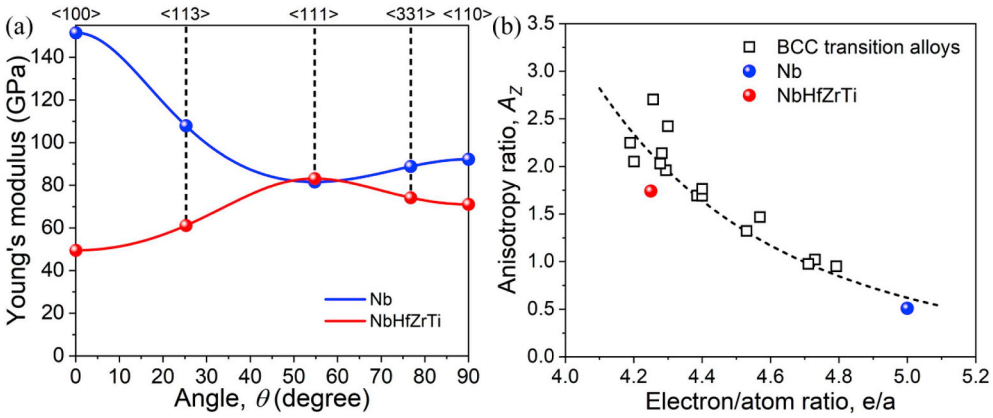

Fig. 4. (a) Young's modulus as a function of crystal direction in the (110) plane showing orientation dependence for pure Nb and NbHfZrTi HEA. (b) Relationship between Zener anisotropy ratio and electron/atom (e/a) ratio for pure Nb, NbHfZrTi HEA, and BCC transition alloys from literature (Ti-Nb [48–51], Ti-Cr [46], and Ti-V [47,52,53] alloys). The dash curve in (b) is drawn to show the trend.

in $A_Z^{HEA} > 1$ and $A_Z^{Nb} < 1$, respectively. It should be noted that the relationship between anisotropy factor and e/a ratio can, in principle, provide a useful guideline to manipulate the elastic anisotropy via compositional adjustment to produce an elastically isotropic HEA [18].

Debye temperature (Θ_D) is one of the fundamental solid-state dynamic parameters that can be deduced from the experimentally/theoretically determined elastic constants, and the standard equation is [54].

$$\Theta_D = \frac{h}{k_B}\left(\frac{3}{4\pi V_a}\right)^{1/3} \upsilon_m \tag{10}$$

where h is Planck's constant, k_B is Boltzmann's constant, $V_a = a^3/2$ is the atomic volume for a BCC crystal and is determined from our previous XRD results [9,12]. The υ_m in the above equation is the average wave velocity in the polycrystalline material, given by

$$\upsilon_m = \left[\frac{1}{3}\left(\frac{1}{\upsilon_L^3} + \frac{2}{\upsilon_T^3}\right)\right]^{-1/3} \tag{11}$$

where $\upsilon_L = \sqrt{(B + 4G/3)/\rho}$ and $\upsilon_T = \sqrt{G/\rho}$ are respectively the longitudinal and transverse sound velocity, and ρ is density. The resulting parameters and calculated Debye temperature Θ_D are summarized in Table 3. It is readily seen in the table that our theoretical DFT calculations and experimental RUS measurements agree quite well (~within 2%) for the longitudinal, transverse and mean sound velocity, and the Debye temperature. It is also noted that the estimated Debye temperatures ($\Theta_D^{RUS} = 214\ K$ and $\Theta_D^{DFT} = 210\ K$) are slightly lower than that for the corresponding constituent elements Zr (291 K), Hf (252 K) and Nb (275 K), but much lower than that for Ti (420 K) [55]. From the viewpoint of thermodynamics [54], the Debye temperature of an alloy is expected to be lower than its constituents due to the local strain generated by a mismatch of atomic sizes; this is in agreement with our calculations.

Rule-of-mixtures (ROM) has been successfully applied to predict the elastic moduli of multi-component alloy systems, in particular, metallic glasses (or amorphous alloys) [56]. Since HEAs are also multi-component, ROM is expected to be applicable to HEAs. In fact, Tian et al. [17]

Table 3
Summary of relevant parameters of NbHfZrTi HEA used for the calculation of Debye temperature.

Methods	G (GPa)	B (GPa)	ρ (g/cm^3)	V_a (Å^3)	υ_L(m/s)	υ_T (m/s)	υ_m(m/s)	Θ_D (K)
RUS	25.1	105.7	8.32	20.42	4090	1737	1964	214
DFT	24.2 (−4%)	112.0 (6%)	8.32	20.42	4164 (2%)	1706 (−2%)	1930 (−2%)	210 (−2%)

Table 4
Material parameters [38,57] used for the rule-of-mixtures (ROM) calculations of equiatomic solid-solution alloys.

Elements	E (GPa)	G (GPa)	B (GPa)	V (cm^3)
Ti	116	44	110	10.64
V	128	47	160	8.32
Cr	279	115	160	7.23
Mn	198	80.8	120	7.35
Fe	211	82	170	7.09
Co	209	75	180	6.67
Ni	200	76	180	6.59
Zr	68	33	91	14.02
Nb	105	38	170	10.83
Mo	329	20	230	9.38
Hf	78	30	110	13.44
Ta	186	69	200	10.85
W	411	161	310	9.47

recently conducted DFT calculations and compared the results with the ROM predictions. They found elastic constants obtained from the two methods agreed reasonably well. However, in another study [21], results showed that, whereas bulk and shear moduli seemed to be in good agreement, Young's modulus appeared to deviate significantly from the ROM prediction. Consequently, in the current study, we also carried out the ROM analysis and compared with experiments as follows.

According to ROM, the elastic moduli, M (E, G or B), of HEAs can be estimated using equations [56].

$$M = \frac{\sum c_i V_i M_i}{\sum c_i V_i} \tag{12}$$

or

$$M^{-1} = \frac{\sum c_i V_i M_1^{-1}}{\sum c_i V_i} \tag{13}$$

where c_i, V_i and M_i are respectively atomic fraction, molar volume and moduli of constituent elements [38,57] (summarized in Table 4). Noted that Eqs. (12) and (13) represent the upper and lower bound values, respectively. To give a broader perspective, in addition to the experimentally measured elastic moduli (E, G and B) of the current alloy, available literature data for other equiatomic single-phase, solid-solution alloys [6,7,22,58–63] are all listed in Table 5. For easy comparison, ROM predictions using both Eqs. (12) and (13) are included in Table 5, and plotted in Fig. 5. It is apparent that ROM based on the lower-bound prediction, Eq. (13) ($R^2 = 0.91$ in Fig. 5b), fits slightly better ($M_{ROM} = M_{Exp.}$) than that based on the upper-bound prediction, Eq. (12) ($R^2 = 0.85$ in Fig. 5a). Data variation from the predictions is evident, especially for the BCC-structured NbMoTaWTi and NbMoTaWTiV, in which the constituent elements have significantly different moduli (Table 4). Nevertheless, results in Fig. 5 suggest that ROM (Eq. (13)) is a practical tool to estimate the elastic moduli of a HEA with either single-phase FCC or BCC structure. However, it is necessary to point out that, despite the usefulness of such a simplistic method, certain factors like chemical interactions among constituent elements and lattice distortion in HEAs are ignored, although they may play a secondary role on elastic moduli.

4. Conclusions

In this study, elastic constants of the single-phase BCC-NbHfZrTi HEA are experimentally measured using resonant ultrasonic spectroscopy (RUS) and also theoretically calculated using the DFT method. Elastic moduli, such as Young's modulus (69.7/67.7 GPa), shear modulus (25.1/24.2 GPa), bulk modulus (105.7/112 GPa) and the Poisson's ratio (0.39/0.40), and the Debye temperature (214/210 K) for

Table 5
Summary of elastic moduli (E, G and B) in a unit of GPa from available experimental measurements using ultrasound methods and ROM predictions. Suffixes u and l denote upper and lower bound predictions using Eqs. (12) and (13), respectively.

Alloys	E (Exp.)	E_u	E_l	G (Exp.)	G_u	G_l	B (Exp.)	B_u	B_l
NbHfZrTi[a]	69.7	89.4	85.3	25.1	35.7	34.9	105.7	117.8	112.0
NbTaHfZrTi [22][b]	78.5	106.9	94.6	28	41.7	38.4	134.6	132.7	121.8
NbMoTaWTi [7][a]	156	222.2	167.9	59	65.3	42.2	139	200.8	178.9
NbMoTaWTiV [7][a]	164	209.0	160.9	62	62.7	42.8	150	195.1	176
NiCoCrFeMn [6][a]	201.6	219.9	216.3	80	86.1	84	140.0	161.2	157.5
NiCoCrFeMn [58][a]	202	219.9	216.3	80	86.1	84	143	161.2	157.5
NiCoCrFeMn [59][a]	202.2	219.9	216.3	80.2	86.1	84	143.8	161.2	157.5
NiCoFeCr [6][a]	215.0	225.7	221.7	84	87.5	84.9	162.9	172.2	171.8
NiCoFeCr [60][b]	204	225.7	221.7	79	87.5	84.9	163	172.2	171.8
NiCoFeMn [6][a]	187.9	204.5	204.3	77	78.6	78.4	111.8	161.5	156.8
NiCoCrMn [6][a]	195.0	222.1	217.7	78	87.2	84.5	130.0	159.0	154.6
NiCoFe [6][a]	162.0	206.8	206.7	60	77.8	77.6	180.0	174.4	164.8
NiCoFe [61][b]	174	206.8	206.7	60	77.8	77.6	177	174.4	164.8
NiCoCr [6][a]	226.2	230.8	225.7	87	89.4	85.9	188.5	172.9	172.4
NiCoCr [62][a]	222	230.8	225.7	85.4	89.4	85.9	185	172.9	172.4
NiCoCr [63][a]	229	230.8	225.7	87.4	89.4	85.9	200.9	172.9	172.4
NiCoCr [61][b]	234	230.8	225.7	87	89.4	85.9	187	172.9	172.4
NiFeMn [6][a]	181.0	203.0	202.8	73	79.7	79.6	116.1	155.7	150.7
NiCoMn [6][a]	189.4	202.2	202.1	77	77.4	77.3	116.9	158.6	152.8
NiCo [6][a]	216.7	204.5	204.4	84	75.5	75.5	172.0	180.0	180
NiFe [6][a]	166.2	205.7	205.5	62	79.1	79	173.1	174.8	174.7

[a] Resonant ultrasound spectroscopy (RUS).
[b] Ultrasonic pulse-echo technique.

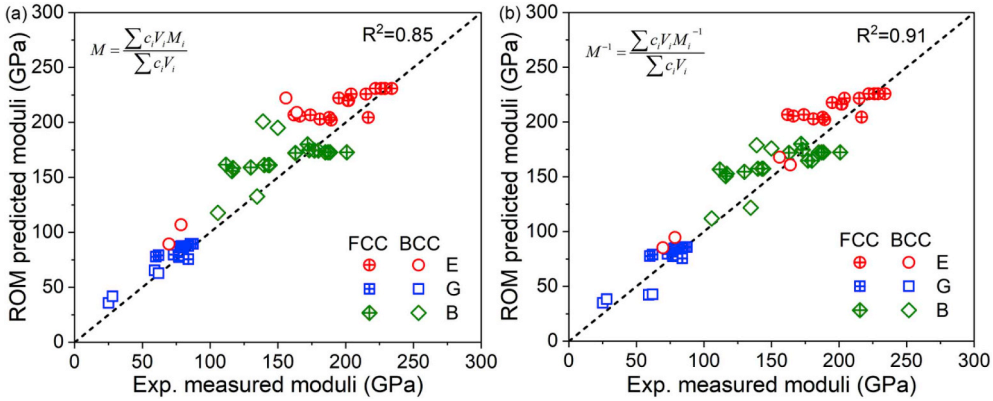

Fig. 5. Comparison of polycrystalline moduli (*E, G* and *B*) of HEAs between ROM predictions and available experimental data. (a) Upper-bound predictions and (b) lower-bound predictions.

polycrystalline aggregates are obtained from the measured and calculated elastic constants. It was found that our RUS experiments and DFT calculations are in excellent agreement (within 6%). The current BCC-NbHfZrTi HEA exhibits a large Pugh's ratio (4.2/4.6), high Poisson's ratio (0.39/0.4), and a positive Cauchy pressure. These elastic properties all affirm that the alloy is ductile, which is actually consistent with reported result [40]. The elastic anisotropy of the alloy is characterized by the Zener ratio (1.74) and 3D visualizations of moduli. Additionally, we have evaluated the applicability of the rule-of-mixtures method to predict the moduli and found that the lower-bond approach is an appropriate way to estimate the elastic moduli of single-phase HEAs with decent precision.

Acknowledgement

This work was supported by the National Science Foundation under Contract NSF DMR-1408722. Y.X.Ye and B.L. Musico would also like to acknowledge funding from the State of Tennessee and Tennessee Higher Education Commission (THEC) through their support of the Center for Materials Processing (CMP). L.B. Xu and H.X. Xu acknowledge NSF DMR-1654438 for the funding support and utilize computational resources at Extreme Science and Engineering Discovery Environment (XSEDE) through TG-DMR170112.

References

[1] J.W. Yeh, S.K. Chen, S.J. Lin, J.Y. Gan, T.S. Chin, T.T. Shun, C.H. Tsau, S.Y. Chang, Nanostructured high-entropy alloys with multiple principal elements: novel alloy design concepts and outcomes, Adv. Eng. Mater. 6 (2004) 299–303.
[2] B. Cantor, I.T.H. Chang, P. Knight, A.J.B. Vincent, Microstructural development in equiatomic multicomponent alloys, Mater. Sci. Eng., A 375 (2004) 213–218.
[3] D.B. Miracle, O.N. Senkov, A critical review of high entropy alloys and related concepts, Acta Mater. 122 (2017) 448–511.
[4] B. Gludovatz, A. Hohenwarter, D. Catoor, E.H. Chang, E.P. George, R.O. Ritchie, A fracture-resistant high-entropy alloy for cryogenic applications, Science 345 (2014) 1153–1158.
[5] X.D. Xu, P. Liu, Z. Tang, A. Hirata, S.X. Song, T.G. Nieh, P.K. Liaw, C.T. Liu, M.W. Chen, Transmission electron microscopy characterization of dislocation structure in a face-centered cubic high-entropy alloy $Al_{0.1}$CoCrFeNi, Acta Mater. 144 (2018) 107–115.
[6] Z. Wu, H. Bei, G.M. Pharr, E.P. George, Temperature dependence of the mechanical properties of equiatomic solid solution alloys with face-centered cubic crystal structures, Acta Mater. 81 (2014) 428–441.
[7] Z.D. Han, N. Chen, S.F. Zhao, L.W. Fan, G.N. Yang, Y. Shao, K.F. Yao, Effect of Ti additions on mechanical properties of NbMoTaW and VNbMoTaW refractory high entropy alloys, Intermetallics 84 (2017) 153–157.
[8] O.N. Senkov, G.B. Wilks, J.M. Scott, D.B. Miracle, Mechanical properties of $Nb_{25}Mo_{25}Ta_{25}W_{25}$ and $V_{20}Nb_{20}Mo_{20}Ta_{20}W_{20}$ refractory high entropy alloys, Intermetallics 19 (2011) 698–706.
[9] Y.X. Ye, Z.P. Lu, T.G. Nieh, Dislocation nucleation during nanoindentation in a body-centered cubic TiZrHfNb high-entropy alloy, Scripta Mater. 130 (2017) 64–68.
[10] Z. Li, K.G. Pradeep, Y. Deng, D. Raabe, C.C. Tasan, Metastable high-entropy dual-phase alloys overcome the strength–ductility trade-off, Nature 534 (2016) 227–230.
[11] Z. Lei, X. Liu, Y. Wu, H. Wang, S. Jiang, S. Wang, X. Hui, Y. Wu, B. Gault, P. Kontis, D. Raabe, L. Gu, Q. Zhang, H. Chen, H. Wang, J. Liu, K. An, Q. Zeng, T.-G. Nieh, Z. Lu, Enhanced strength and ductility in a high-entropy alloy via ordered oxygen complexes, Nature 563 (2018) 546–550.
[12] Y.X. Ye, C.Z. Liu, H. Wang, T.G. Nieh, Friction and wear behavior of a single-phase equiatomic TiZrHfNb high-entropy alloy studied using a nanoscratch technique, Acta Mater. 147 (2018) 78–89.
[13] T. Zuo, M. Zhang, P.K. Liaw, Y. Zhang, Novel high entropy alloys of Fe_xCo_{1-x} NiMnGa with excellent soft magnetic properties, Intermetallics 100 (2018) 1–8.
[14] S. Huang, F. Tian, L. Vitos, Elasticity of high-entropy alloys from ab initio theory, J. Mater. Res. 33 (2018) 2938–2953.
[15] H. Zhang, X. Sun, S. Lu, Z. Dong, X. Ding, Y. Wang, L. Vitos, Elastic properties of $Al_xCrMnFeCoNi$ ($0 \le x \le 5$) high-entropy alloys from ab initio theory, Acta Mater. 155 (2018) 12–22.
[16] H. Ge, H. Song, J. Shen, F. Tian, Effect of alloying on the thermal-elastic properties of 3d high-entropy alloys, Mater. Chem. Phys. 210 (2018) 320–326.
[17] L.-Y. Tian, G. Wang, J.S. Harris, D.L. Irving, J. Zhao, L. Vitos, Alloying effect on the elastic properties of refractory high-entropy alloys, Mater. Des. 114 (2017) 243–252.
[18] F. Tian, L.K. Varga, N. Chen, J. Shen, L. Vitos, Ab initio design of elastically isotropic $TiZrNbMoV_x$ high-entropy alloys, J. Alloy. Comp. 599 (2014) 19–25.
[19] M. Liao, Y. Liu, L. Min, Z. Lai, T. Han, D. Yang, J. Zhu, Alloying effect on phase stability, elastic and thermodynamic properties of Nb-Ti-V-Zr high entropy alloy, Intermetallics 101 (2018) 152–164.
[20] S. Qiu, N. Miao, J. Zhou, Z. Guo, Z. Sun, Strengthening mechanism of aluminum on elastic properties of NbVTiZr high-entropy alloys, Intermetallics 92 (2018) 7–14.
[21] Z. Wen, Y. Zhao, J. Tian, S. Wang, Q. Guo, H. Hou, Computation of stability, elasticity and thermodynamics in equiatomic AlCrFeNi medium-entropy alloys, J. Mater. Sci. 54 (2018) 2566–2576.
[22] G. Dirras, L. Lilensten, P. Djemia, M. Laurent-Brocq, D. Tingaud, J.-P. Couzinié, L. Perrière, T. Chauveau, I. Guillot, Elastic and plastic properties of as-cast equimolar TiHfZrTaNb high-entropy alloy, Mater. Sci. Eng., A 654 (2016) 30–38.
[23] A. Migliori, J.L. Sarrao, Resonant Ultrasound Spectroscopy: Applications to Physics, Materials Measurements, and Nondestructive Evaluation, Wiley, New York, 1997.
[24] P. Hohenberg, W. Kohn, Inhomogeneous electron gas, Phys. Rev. 136 (1964) B864.
[25] W. Kohn, L.J. Sham, Self-consistent equations including exchange and correlation effects, Phys. Rev. 140 (1965) A1133.
[26] G. Kresse, J. Furthmüller, Efficiency of ab-initio total energy calculations for metals and semiconductors using a plane-wave basis set, Comput. Mater. Sci. 6 (1996) 15–50.
[27] G. Kresse, J. Hafner, Ab initio molecular dynamics for liquid metals, Phys. Rev. B 47 (1993) 558.
[28] P.E. Blöchl, Projector augmented-wave method, Phys. Rev. B 50 (1994) 17953.
[29] J.P. Perdew, K. Burke, M. Ernzerhof, Generalized gradient approximation made simple, Phys. Rev. Lett. 77 (1996) 3865.
[30] A. Zunger, S.-H. Wei, L. Ferreira, J.E. Bernard, Special quasirandom structures, Phys. Rev. Lett. 65 (1990) 353.
[31] A. Van de Walle, P. Tiwary, M. De Jong, D. Olmsted, M. Asta, A. Dick, D. Shin, Y. Wang, L.-Q. Chen, Z.-K. Liu, Efficient stochastic generation of special quasirandom structures, Calphad 42 (2013) 13–18.
[32] A. Van De Walle, M. Asta, G. Ceder, The alloy theoretic automated toolkit: a user guide, Calphad 26 (2002) 539–553.
[33] A. van de Walle, Multicomponent multisublattice alloys, nonconfigurational entropy and other additions to the Alloy Theoretic Automated Toolkit, Calphad 33 (2009) 266–278.
[34] Y. Le Page, P. Saxe, Symmetry-general least-squares extraction of elastic data for strained materials from ab initio calculations of stress, Phys. Rev. B 65 (2002) 104104.
[35] X. Wu, D. Vanderbilt, D. Hamann, Systematic treatment of displacements, strains, and electric fields in density-functional perturbation theory, Phys. Rev. B 72 (2005) 035105.
[36] J.F. Nye, Physical Properties of Crystals: Their Representation by Tensors and

Matrices, Oxford university press, 1985.
[37] R. Hill, The elastic behaviour of a crystalline aggregate, Proc. Phys. Soc. 65 (1952) 349.
[38] S. Pugh, XCII. Relations between the elastic moduli and the plastic properties of polycrystalline pure metals, Lond. Edinb. Dublin Philos. Mag. J. Sci. 45 (1954) 823–843.
[39] D. Pettifor, Theoretical predictions of structure and related properties of intermetallics, Mater. Sci. Technol. 8 (1992) 345–349.
[40] Y.D. Wu, Y.H. Cai, T. Wang, J.J. Si, J. Zhu, Y.D. Wang, X.D. Hui, A refractory $Hf_{25}Nb_{25}Ti_{25}Zr_{25}$ high-entropy alloy with excellent structural stability and tensile properties, Mater. Lett. 130 (2014) 277–280.
[41] J. Li, K.J. Van Vliet, T. Zhu, S. Yip, S. Suresh, Atomistic mechanisms governing elastic limit and incipient plasticity in crystals, Nature 418 (2002) 307.
[42] V. Tvergaard, J.W. Hutchinson, Microcracking in ceramics induced by thermal expansion or elastic anisotropy, J. Am. Ceram. Soc. 71 (1988) 157–166.
[43] J. Wortman, R. Evans, Young's modulus, shear modulus, and Poisson's ratio in silicon and germanium, J. Appl. Phys. 36 (1965) 153–156.
[44] W. Brantley, Calculated elastic constants for stress problems associated with semiconductor devices, J. Appl. Phys. 44 (1973) 534–535.
[45] D. Bolef, Elastic constants of single crystals of the bcc transition elements V, Nb, and Ta, J. Appl. Phys. 32 (1961) 100–105.
[46] E.S. Fisher, D. Dever, Relation of the C' elastic modulus to stability of bcc transition metals, Acta Metall. 18 (1970) 265–269.
[47] K.W. Katahara, M.H. Manghnani, E.S. Fisher, Pressure derivatives of the elastic moduli of BCC Ti-V-Cr, Nb-Mo and Ta-W alloys, J. Phys. F Met. Phys. 9 (1979) 773–790.
[48] M. Tane, S. Akita, T. Nakano, K. Hagihara, Y. Umakoshi, M. Niinomi, H. Nakajima, Peculiar elastic behavior of Ti–Nb–Ta–Zr single crystals, Acta Mater. 56 (2008) 2856–2863.
[49] R. Hermann, H. Hermann, M. Calin, B. Büchner, J. Eckert, Elastic constants of single crystalline β-Ti70Nb30, Scripta Mater. 66 (2012) 198–201.
[50] C.N. Reid, J.L. Routbort, R.A. Maynard, Elastic constants of Ti–40 at.% Nb at 298 °K, J. Appl. Phys. 44 (1973) 1398–1399.
[51] H.W. Jeong, Y.S. Yoo, Y.T. Lee, J.K. Park, Elastic softening behavior of Ti–Nb single crystal near martensitic transformation temperature, J. Appl. Phys. 108 (2010) 063515.
[52] L.A. Ahlberg, O. Buck, N.E. Paton, Effects of hydrogen on anisotropic elastic properties of bcc Ti-alloys, Scripta Metall. 12 (1978) 1051–1054.
[53] E.S. Fisher, Physics of Solid Solution Strengthening, Plenum Press, New York, 1975.
[54] A. Teklu, H. Ledbetter, S. Kim, L. Boatner, M. McGuire, V. Keppens, Single-crystal elastic constants of Fe-15Ni-15Cr alloy, Metall. Mater. Trans. 35 (2004) 3149–3154.
[55] C. Kittel, Introduction to Solid State Physics, Wiley, 2005.
[56] W.H. Wang, The elastic properties, elastic models and elastic perspectives of metallic glasses, Prog. Mater. Sci. 57 (2012) 487–656.
[57] M.J. Winter, WebElements: the periodic table of the elements, http://www.webelements.com, (2015).
[58] A. Haglund, M. Koehler, D. Catoor, E. George, V. Keppens, Polycrystalline elastic moduli of a high-entropy alloy at cryogenic temperatures, Intermetallics 58 (2015) 62–64.
[59] K. Tanaka, T. Teramoto, R. Ito, Monocrystalline elastic constants of fcc-CrMnFeCoNi high entropy alloy, MRS Adv. 2 (2017) 1429–1434.
[60] A. Vida, L.K. Varga, N.Q. Chinh, D. Molnar, S. Huang, L. Vitos, Effects of the sp element additions on the microstructure and mechanical properties of NiCoFeCr based high entropy alloys, Mater. Sci. Eng., A 669 (2016) 14–19.
[61] K. Jin, Y. Gao, H. Bei, Intrinsic properties and strengthening mechanism of monocrystalline Ni-containing ternary concentrated solid solutions, Mater. Sci. Eng., A 695 (2017) 74–79.
[62] I. Moravcik, J. Cizek, Z. Kovacova, J. Nejezchlebova, M. Kitzmantel, E. Neubauer, I. Kubena, V. Hornik, I. Dlouhy, Mechanical and microstructural characterization of powder metallurgy CoCrNi medium entropy alloy, Mater. Sci. Eng., A 701 (2017) 370–380.
[63] B. Gludovatz, A. Hohenwarter, K.V. Thurston, H. Bei, Z. Wu, E.P. George, R.O. Ritchie, Exceptional damage-tolerance of a medium-entropy alloy CrCoNi at cryogenic temperatures, Nat. Commun. 7 (2016) 10602.